Polarization-resolved second-harmonic generation in tendon upon mechanical stretching

Ivan Gusachenko, Viet Tran, Yannick Goulam Houssen, Jean-Marc Allain, Marie-Claire Schanne-Klein

Polarization-Resolved Second-Harmonic Generation in Tendon upon Mechanical Stretching

Ivan Gusachenko,[†‡] Viet Tran,[§] Yannick Goulam Houssen,[†] Jean-Marc Allain,[§] and Marie-Claire Schanne-Klein[†*]
[†]Laboratory for Optics and Biosciences, Ecole Polytechnique, Centre National de la Recherche Scientifique, Institut National de la Santé et de la Recherche Médicale U696, Palaiseau, France; [‡]Laboratory of Cellular Structure Morphology and Function, Siberian Branch of the Russian Academy of Sciences, Institute of Cytology and Genetics, Novosibirsk, Russia; and [§]Solids Mechanics Laboratory, Ecole Polytechnique, Centre National de la Recherche Scientifique, Palaiseau, France

ABSTRACT Collagen is a triple-helical protein that forms various macromolecular organizations in tissues and is responsible for the biomechanical and physical properties of most organs. Second-harmonic generation (SHG) microscopy is a valuable imaging technique to probe collagen fibrillar organization. In this article, we use a multiscale nonlinear optical formalism to bring theoretical evidence that anisotropy of polarization-resolved SHG mostly reflects the micrometer-scale disorder in the collagen fibril distribution. Our theoretical expectations are confirmed by experimental results in rat-tail tendon. To that end, we report what to our knowledge is the first experimental implementation of polarization-resolved SHG microscopy combined with mechanical assays, to simultaneously monitor the biomechanical response of rat-tail tendon at macroscopic scale and the rearrangement of collagen fibrils in this tissue at microscopic scale. These experiments bring direct evidence that tendon stretching corresponds to straightening and aligning of collagen fibrils within the fascicle. We observe a decrease in the SHG anisotropy parameter when the tendon is stretched in a physiological range, in agreement with our numerical simulations. Moreover, these experiments provide a unique measurement of the nonlinear optical response of aligned fibrils. Our data show an excellent agreement with recently published theoretical calculations of the collagen triple helix hyperpolarizability.

INTRODUCTION

Polarization-resolved second-harmonic generation (P-SHG) microscopy has recently emerged as a new multiphoton modality that efficiently probes the three-dimensional architecture of collagenous tissues (1–13). This modality takes advantage of the high specificity of SHG signals for dense noncentrosymmetric macromolecular organizations (14–17) and of the sensitivity of polarimetric approaches to the molecular orientation distribution. It is of great interest for collagenous tissues because of the highly anisotropic organization of fibrillar collagens in tissues. Fibrillar collagens are characterized by a long triple-helical domain and self-assemble to form fibrils with various diameters and distributions depending on the tissue (18). The hierarchical organization of collagen is responsible for the biophysical and mechanical properties of most tissues. For instance, the transparency of cornea results from the almost crystalline order of 30-nm-diameter collagen fibrils within 2-μm-thick stacked lamellas in the corneal stroma. In the same vein, the mechanical strength of tendons results from the many hierarchical levels of collagen organization within this tissue. Tendons are composed of collagen type I that forms $\approx$200-nm-diameter fibrils, which further assemble to form a few μm-diameter fibers and finally around 100 μm-diameter fascicles (19). The latter tissue has been extensively studied as a model system with uniaxial symmetry because tendon fascicles are easily extracted from rat-tails (1,9,10,12,20).

Analysis of P-SHG images is a complex task in collagenous tissues because of the many parameters involved in the tissular response. Usually, the collagen SHG response is characterized by the SHG anisotropy parameter ρ, which is related to the ratio of the SHG responses when the excitation field is polarized parallel (respectively, perpendicular) to the tendon fascicle axis (1,3,5,6,8,9,11,12). However, the relationship of this parameter to the collagen molecular response and the fibril orientation distribution is not fully characterized yet. Moreover, tendon fascicles exhibit anisotropic linear optical properties, mainly birefringence and diattenuation, which may distort P-SHG data and impede measurements of ρ (1,7,9,10,21).

This article aims to determine the origin of the variations of the SHG anisotropy parameter ρ to serve as a possible probe of the collagen submicrometer-scale organization in various physiological conditions. To that end, we perform P-SHG measurements in rat-tail tendon fascicles subjected to varying mechanical loads. This method enables the characterization of the same tissue while varying the orientational distribution of collagen fibrils because mechanical load results in a rearrangement of the collagen fibrils within the tendon (22–24). In this way, we report what is, to our knowledge, the first experimental observation of ρ-variations in the same region of interest (ROI) of a tendon fascicle upon mechanical loading. We propose a theoretical analysis of these variations by considering collagen fibrils with identical tensorial SHG response but

Submitted December 14, 2011, and accepted for publication March 23, 2012.

*Correspondence: marie-claire.schanne-klein@polytechnique.edu

Editor: Gijsje Koenderink.

0006-3495/12/05/2220/10 $2.00

doi: 10.1016/j.bpj.2012.03.068

varying orientational distribution. We also carefully process our images to correct for artifacts related to linear optical anisotropy of tendon fascicles. We obtain a good agreement between experimental data and theoretical calculations, which indicates that variations of the SHG anisotropy parameter ρ are mainly due to a rearrangement of the fibril orientational distribution within the tissue.

In the following, we first present our experimental setup that combines a traction device with a P-SHG microscope. Then, we propose a theoretical approach to gain insight into the origin of the variation of the SHG anisotropy parameter ρ. Next, we present three-dimensional P-SHG images of tendon fascicles under mechanical loading and determine the variation of linear birefringence, diattenuation, and SHG anisotropy parameter ρ as a function of the fascicle strain. Finally, we discuss these results in our theoretical framework, before concluding.

MATERIALS AND METHODS

Tendon preparation

Tendons were extracted from Sprague-Dawley rat-tails (female, ≈300 g) that were kept frozen until dissection. The fascicles were rinsed in phosphate-buffered saline (PBS) and centrifugated at 4700 rpm to remove any other tissue components, as described previously (24). They were stored at 4° in PBS and used within a few days for the experiments. Tendon fascicles were first labeled with fluorescent latex beads (1-μm diameter, L1030; Sigma-Aldrich, St. Louis, MO) to enable precise localization of the tissue surface. They were then attached to the traction device by use of metallic plates with rod-shaped inserts. They were coiled on the rods in a symmetric manner and glued with cyanoacrylate on the metallic plates. Before mounting in the stretching device, they were suspended vertically and allowed to rotate freely so as to minimize initial torsion. The plates were then screwed to the testing device and immersed in a dish filled with PBS to prevent the tendon fascicle from drying. The bottom of the dish consisted of a glass coverslip to enable *trans*-detection of SHG signals (see Fig. 1).

Polarization-resolved multiphoton microscopy

Multiphoton imaging was performed using a custom-built laser-scanning upright microscope as previously described (9,16). Briefly, excitation was provided by a femtosecond Titanium-sapphire laser tuned at 860 nm (Tsunami; Spectra-Physics, Tucson, AZ), which was focused using a water-immersion 20×, 0.95 NA objective with resolution typically 0.4 μm (lateral) × 1.6 μm (axial) near the sample surface. Multiphoton signals were collected with photon-counting photomultiplier tubes (P25PC; ET Enterprise, Uxbridge, United Kingdom) using appropriate dichroic mirrors and spectral filters as depicted in Fig. 1. 2PEF was detected in the backward direction and SHG either in the forward or backward directions. Multimodal images were usually recorded using 200 kHz pixel rate, 0.8 μm pixel size, and 2 μm z-step, with 15–20 mW excitation power at the focus. No degradation of the tendon fascicle was observed under these conditions.

Polarization-resolved imaging was achieved by tuning the polarization of the laser excitation and analyzing the forward SHG (F-SHG) signals (9). To that end, we inserted a linear infrared polarizer at the back pupil of the objective to correct the nonnegligible ellipticity of the excitation beam due to the optical components within the microscope. We thereby achieved a linear polarization with ellipticity <1% at small scanning

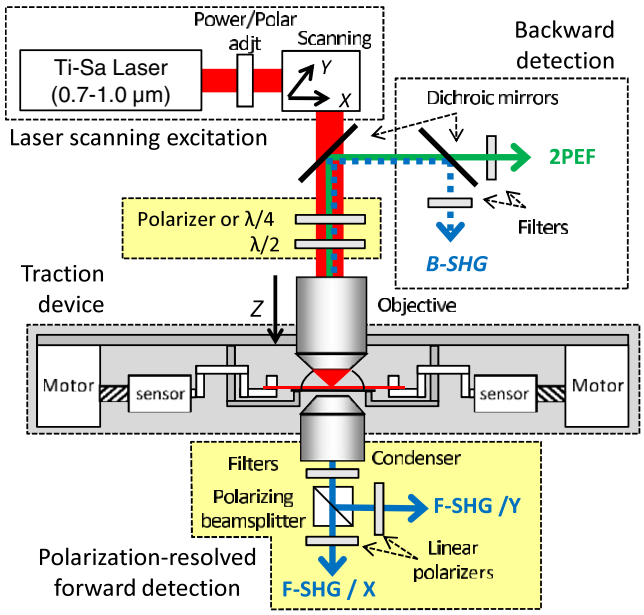

FIGURE 1 Laser-scanning multiphoton microscope with polarization-resolved detection of F-SHG signal and epi-detection of 2PEF signal and possibly of B-SHG signal. The symmetrical traction device is inserted between the objective and the condenser, with a glass window below the tendon fascicle.

angles. This linear polarization was tuned from $-2\pi/3$ to $2\pi/3$ (usually with $\pi/12$ steps) by rotating an achromatic half-wave plate (MWPAA2-22-700-1000; CVI-Melles Griot, Albuquerque, NM) placed just before the objective (see Fig. 1). F-SHG signals were analyzed using a polarizing beamsplitter cube (BBPC-550; CVI-Melles Griot). The extinction ratio of the x- and y-polarized detection channels was maximized by putting linear polarizers (03FPG021; CVI-Melles Griot) in front of the detectors. The relative transmission of these two channels was calibrated using a fluorescent slide before each experiment to enable quantitative comparison between x- and y-polarized F-SHG images (9). Image processing was performed using MATLAB (The MathWorks, Natick, MA) and ImageJ (W. Rasband, National Institutes of Health, Bethesda, MD) softwares with the MIJ plug-in (25).

Traction device and loading path

The traction device was a custom-built uniaxial device designed to stretch the tendon fascicles in a symmetrical way to enable continuous imaging of the same region at the center of the fascicle. This device was composed of two motors (drl42pa2g-04; Oriental Motor, Tokyo, Japan) and two force sensors (k1563-100N; Annemasse, France) on both sides of the fascicle (see Fig. 1). Force and displacement were measured every 1 s. This device was inserted in place of the microscope stage, so that the tendon fascicle was imaged in an upright geometry, with F-SHG signals collected by a condenser lens just below the coverslip glass window of the PBS-filled dish. Multiphoton imaging was first performed continuously to adjust the position of the fascicle at the beam focus. The fascicles were then stretched until the crimps disappeared, and slightly relaxed to observe again the crimps. This position was referred as the zero strain, and the corresponding length of the fascicle as the reference length l_0 (24). Strain was then obtained as the ratio of the total metallic plates displacement divided by this reference length (typically 40 mm). It could be slightly overestimated because of the uncertainty in the zero strain position, but the relative strain values were accurately determined.

Combined SHG imaging and mechanical assay were performed as follows. We increasingly stretched the fascicles at 10 μm/s constant strain rate by steps of 1% strain. At each step, we stopped the motors and waited ~10 min until the fascicle relaxed to a quasistatic state. We then recorded z-stacks of multiphoton images in immobilized fascicle. We verified that we always imaged the same region of the fascicle by looking at characteristic patterns from fluorescent beads on the fascicle. When necessary, we slightly adjusted the lateral and axial positions of the fascicle by moving the whole traction device by mean of micrometer stages. P-SHG imaging was then performed in a 20 μm $\times$ 28 μm ROI at the center of the fascicle.

We carried out measurements in seven stretched tendons; three of them were preconditioned by stretching directly to 6–8% and then relaxing until crimps were again observed (typically 2–4% strain instead of zero because of hysteresis). No significant behavior difference was observed between preconditioned and nonpreconditioned tendons.

THEORETICAL BACKGROUND

Second-harmonic generation in tendon

SHG is usually described using second-order nonlinear optical susceptibility tensor $\chi^{(2)}$. In this formalism, the nonlinear optical polarization at the harmonic frequency 2ω, induced by an incident electric field $\mathbf{E}$ at frequency ω in a uniform medium, is given by

$$P_i = \chi^{(2)}_{ijk} E_j E_k. \quad (1)$$

It is nonzero only in noncentrosymmetric media. Tendon fascicle are commonly assumed to have cylindrical symmetry (1,20), which reduces the number of independent nonvanishing tensorial components of $\chi^{(2)}$. Moreover, we assume that Kleinman symmetry applies because of the nonresonant character of the interaction (1,20). Within these assumptions, $\chi^{(2)}$ has only two independent nonvanishing components: χ_{xxx} and $\chi_{xyy} = \chi_{yxy} = \chi_{yyx} = \chi_{xzz} = \chi_{zxz} = \chi_{zzx}$, where x is the main axis of the tendon fascicle (1,20). P-SHG experiments give access to the ratio of these tensor components: $\rho = \chi_{xxx}/\chi_{xyy}$. This SHG anisotropy parameter measures the ratio of the SHG responses when the incident electric field is parallel (respectively, perpendicular) to the tendon axis.

Collagen hierarchical structure and orientational disorder in tendon

The nonlinear susceptibility tensor $\chi^{(2)}$ represents the macroscopic nonlinear response of the medium that is composed of elementary scatterers at a smaller scale. These elementary responses are described by a first hyperpolarizability tensor (26). The very elementary nonlinear scatterers in collagenous tissues are presumably the peptide bonds along the peptidic scaffold (3,27). These molecular entities present delocalized electrons in a noncentrosymmetric environment, which gives a nonvanishing second-harmonic response. Moreover, they are tightly aligned along the collagen triple helices and within the fibrils and fascicles, so that their small second-harmonic responses are coherently amplified and the resulting macroscopic response $\chi^{(2)}$ is quite large (27).

Considering the hierarchical organization of collagen, one may define hyperpolarizability tensors at different scales: peptide bonds, triple helices, or fibrils (see Fig. 2 *a*). In this work, we assume that collagen triple helices and fibrils are quite rigid upon physiological mechanical loads, which means that physiological mechanical deformations are only accompanied with reorganization of fibrils within the fascicle. We therefore consider collagen fibrils as the relevant elementary nonlinear optical structure at submicrometer scale. Within this assumption, all the collagen fibrils exhibit the same first hyperpolarizability tensor β in their associated reference frames, but they show orientational dispersion around the fascicle main axis. Because the macroscopic SH polarization is obtained as the sum of elementary nonlinear dipole moments, the susceptibility tensor reads

$$\chi^{(2)}_{ijk} = N\left\langle \beta^{(2)}_{ijk} \right\rangle_{\Omega}, \quad (2)$$

where N is the fibril concentration and the average is taken over the angular distribution Ω of fibrils. Local field factors have been neglected in this expression.

The fibrils are assumed to exhibit cylindrical symmetry like the fascicles, so that the nonzero hyperpolarizability

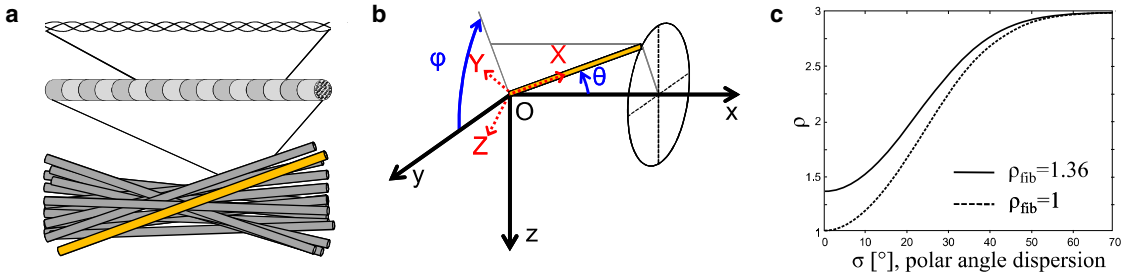

FIGURE 2 Orientational disorder in tendon. (*a*) Hierarchical structure of collagen, from molecule to fibril and fascicle. P-SHG probes the orientational distribution of fibrils within the fascicle. (*b*) Collagen fibril with (θ,φ) orientation. (x,y,z) and (X,Y,Z) denote laboratory frame and fibril frame, respectively. (*c*) Effective SHG anisotropy parameter ρ as a function of fibril orientation dispersion in the tendon fascicle for fibril parameter $\rho_{\text{fib}} = 1$ and $\rho_{\text{fib}} = 1.36$.

components in the fibril frame are β_{XXX} and $\beta_{XYY} = \beta_{YXY} = \beta_{YYX} = \beta_{XZZ} = \beta_{ZXZ} = \beta_{ZZX}$ for the same symmetry reasons as for $\chi^{(2)}$. The orientation of such a collagen fibril with cylindrical symmetry can be described by two angles (θ,φ), where θ represents the polar angle between the fibril's main axis X and the x axis in the laboratory frame (Fig. 2 *b*) and φ is the azimuthal angle of the fibril with respect to the xy plane in the laboratory frame. For a single fibril at (θ,φ), the hyperpolarizability in the laboratory frame reads

$$\beta_{ijk} = \sum_{I,J,K} T_{iI}T_{jJ}T_{kK}\beta_{IJK}, \tag{3}$$

where (i,j,k) and (I,J,K) denote coordinates in the laboratory frame and in the fibril frame, respectively, and T is the Euler matrix (see the Supporting Material).

Moreover, at a smaller scale, the hyperpolarizability tensor of a collagen fibril can be related to the elementary hyperpolarizability tensor of a peptide bond $\tilde{\beta}$ using an expression similar to Eq. 3,

$$\beta_{IJK} = \sum_{a,b,c} T_{Ia}T_{Jb}T_{Kc}\tilde{\beta}_{abc}, \tag{4}$$

where (a,b,c) and (I,J,K) denote coordinates in the peptide frame and in the fibril frame, respectively. It is usually assumed that the peptide bonds behave as rodlike nonlinear scatterers so that there is only one nonvanishing component $\tilde{\beta}_{uuu}$ (3).

To summarize, we consider the nonlinear optical response of collagen at three different scales: the very elementary scale $\tilde{\beta}$ that corresponds to the peptide bonds, the fibrils scale β, and the tissue scale $\chi^{(2)}$ that is probed through imaging or spectroscopic experiments. As stated above, this three-scale approach aims to separate the scale of the fibrils that are considered as rigid entities from the scale of the tissue where the fibrils distribution may vary dramatically upon various perturbations.

SHG anisotropy parameter at fibrillar and tissular scales

In the following, we further consider that fibrils are uniformly distributed around the x axis, with an orientational distribution

$$F(\theta,\varphi) = \frac{1}{2\pi}g(\theta),$$

where $g(\theta)$ is an appropriate distribution density function of θ. Using this distribution and Eqs. 2 and 3, the relationship between the macroscopic nonlinear response $\chi^{(2)}$ and fibril first hyperpolarizability β reads

$$\chi^{(2)}_{xxx} = N\beta_{XXX}\langle\cos^3\theta\rangle_g + 3N\beta_{XYY}\langle\cos\theta\sin^2\theta\rangle_g, \tag{5}$$

$$\chi^{(2)}_{xyy} = \frac{1}{2}N\left(\beta_{XXX}\langle\cos\theta\sin^2\theta\rangle_g + \beta_{XYY}\left(3\langle\cos^3\theta\rangle_g - \langle\cos\theta\rangle_g\right)\right). \tag{6}$$

The SHG anisotropy parameter ρ is determined from

$$\rho = \frac{\chi^{(2)}_{xxx}}{\chi^{(2)}_{xyy}} = \frac{\rho_{\text{fib}}\langle\cos^3\theta\rangle_g + 3\langle\cos\theta\sin^2\theta\rangle_g}{\frac{3}{2}\langle\cos^3\theta\rangle_g - \frac{1}{2}\langle\cos\theta\rangle_g + \frac{1}{2}\rho_{\text{fib}}\langle\cos\theta\sin^2\theta\rangle_g}, \tag{7}$$

where we have introduced an SHG anisotropy parameter at the scale of a single fibril $\rho_{\text{fib}} = \beta_{XXX}/\beta_{XYY}$.

At a smaller scale, ρ_{fib} may also be related to the angle Θ of the elementary nonlinear scatterers to the fibril axis by deriving a relationship between β_{XXX} (respectively, β_{XYY}) and $\tilde{\beta}_{uuu}$ similarly to Eq. 5 (respectively, Eq. 6). In that case, because there is only one nonvanishing component $\tilde{\beta}_{uuu}$, these expressions simplify to (3,5,6)

$$\beta_{XXX} = N\tilde{\beta}_{uuu}\cos^3\Theta, \tag{8}$$

$$\beta_{XYY} = \frac{1}{2}N\tilde{\beta}_{uuu}\cos\Theta\sin^2\Theta, \tag{9}$$

and ρ_{fib} reads

$$\rho_{\text{fib}} = \frac{\beta_{XXX}}{\beta_{XYY}} = \frac{2}{tg^2(\Theta)}. \tag{10}$$

This expression is strictly valid for a unique orientation Θ of the elementary nonlinear scatterers to the fibril axis. It may be refined considering the accurate geometry of a triple-helix (27,28) and the structure of a fibril (29). It is noteworthy that we consider a rigid structure at this scale. Orientational disorder within the fascicle is only relevant at a larger scale that corresponds to the rearrangement of the fibrils upon stretching, as shown in Eq. 7.

We now focus on the fascicle scale and we examine Eq. 7. It shows that the parameter ρ that is measured using P-SHG experiments is related to the corresponding parameter ρ_{fib} at the fibril scale and to the angular dispersion of the fibrils within the focal volume

$$\sigma = \sqrt{\langle\theta^2\rangle_g}.$$

Given the values of ρ reported in the literature, we expect that $\rho_{\text{fib}} < 3$ for rat-tail tendon fascicle. In that case, the effective parameter ρ increases with σ that is with disorder (see the Supporting Material). The same trend has been reported in the particular case of a conical distribution at a fixed angle θ when increasing θ (12). Calculation of parameter ρ as a function of σ is displayed in Fig. 2 *c* in

the simplified case of a Gaussian distribution around the x axis,

$$g(\theta) \propto e^{-\frac{\theta^2}{2\sigma^2}}$$

(see the Supporting Material). The value ρ monotonically increases with angular dispersion up to 3. For example, ρ is calculated as 1.5 that is a typical value reported in the literature, using a fibril parameter $\rho_{\text{fib}} = 1$ and orientation dispersion as small as 15°. As expected, ρ tends toward ρ_{fib} for σ tending toward zero. Our calculation thus demonstrates unambiguously that the measured SHG anisotropy parameter ρ reflects the orientational disorder of the fibrils within the fascicle.

P-SHG in thick anisotropic tissues

The parameter ρ is measured using P-SHG imaging experiments. Advanced image processing is required to take into account possible polarization distortions due to propagation within the tendon fascicle, as reported in our recent article (9). Laser excitation is indeed affected by diattenuation and birefringence when propagating within this thick anisotropic tissue, while SHG radiation undergoes polarization scrambling. A complete description of our image processing is given as the Supporting Material. Briefly, we fit the SHG signal intensity along x polarization as

$$I^{2\omega}(\alpha) = A\cos 4\alpha + B\cos 2\alpha + C, \qquad (11)$$

where α is the polarization angle of the incident electric field in the xy plane. The parameter ρ then reads

$$\rho^2 e^{-\frac{2z}{\Delta l}} = \frac{A + B + C}{A - B + C}, \qquad (12)$$

where $\Delta l^{-1} = l_x^{-1} - l_y^{-1}$ is the diattenuation. Diattenuation corresponds to the difference of attenuation lengths for the two orthogonal polarizations of the incident beam: parallel ($\alpha = 0$) and perpendicular ($\alpha = \pi/2$) to the tendon fascicle axis. It can be extracted from experimental data by fitting $I^{2\omega}_{x,\alpha=0}(z)$ and $I^{2\omega}_{x,\alpha=\pi/2}(z)$ z-profiles using exponential functions. Finally, we calculate a second parameter Δ from A,B,C (see the Supporting Material) to extract the birefringence Δn and the amount of polarization scrambling $\eta(z_0)$ near the tendon surface. This advanced data analysis method thus enables the determination of both linear and nonlinear optical properties in any ROI of the tendon fascicle.

RESULTS

Mechanical assays

We performed mechanical assays coupled with P-SHG measurements in tendon fascicles to characterize the variation of the collagen organization under mechanical load. A typical loading path is displayed in Fig. 3, along with force measurements that show a relaxation while the strain is kept constant. We therefore always recorded SHG image stacks after ~10-min relaxation, to probe the fascicle in a quasi-steady state. The imaging recording time is quite long (typically 3 min; see *boxes* in Fig. 3 *a*) because many images (typically 850) are recorded to retrieve the polarization dependence at increasing depths within the fascicle.

The force-strain response of the tendon fascicle is displayed in Fig. 3 *b*. The force shows a slow continuous increase superimposed to steep variations related to fascicle relaxation while motors are immobile. The variation of the fascicle stiffness (slope of the force-strain curve) as measured between two successive steps with increasing strain is in good agreement with previously reported data (24,30). A toe region with increasing stiffness is observed below 3% strain. Then the fascicle exhibits a linear behavior with constant stiffness (3–6% strain). The tangent modulus is ~200 MPa in this region, similarly to the values reported for fascicles in the literature (24,31,32). Finally, the stiffness decreases, indicating that force saturates at strains beyond 6%, which shows that the fascicle begins to break.

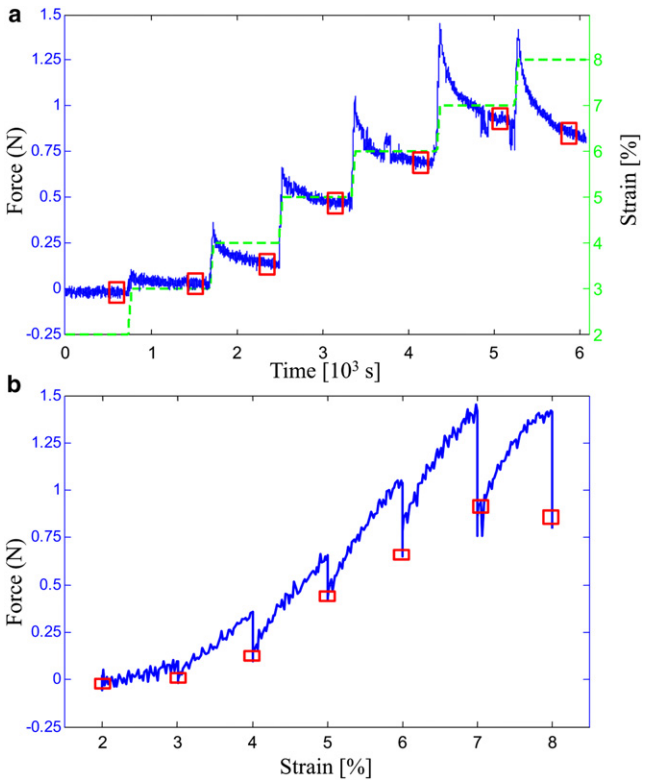

FIGURE 3 Mechanical behavior of a tendon fascicle. (*a*) Loading path of the mechanical assay (strain as a function of time, *dotted line*) and response of the tendon fascicle (force as a function of time, *solid line*). (*Rectangles*) Times when P-SHG imaging was performed. (*b*) Force variation as a function of strain along the loading path. Negative peaks at integer values correspond to tendon mechanical relaxation while motors are stopped.

P-SHG images of tendon fascicle

Fig. 4 displays P-SHG imaging data from the same fascicle at 2% and 4% strains. SHG images exhibit a striated pattern that is characteristic for the collagen fibrillar organization in tendon fascicles (1,2,4,24) (see Fig. 4, *a* and *e*). It does not directly reproduce the fibril distribution within the fascicle, but corresponds to interference patterns resulting from the coherent summation of the SHG radiation from all the fibrils within the focal volume (33–35). We used simultaneous 2PEF imaging to visualize fluorescent beads that labeled the fascicle surface. We observed the same bead patterns at any strain, which indicates that we successfully imaged the same region of the fascicle thanks to symmetric stretching in our traction device. Slight displacements of this pattern between two successive strains were sometimes observed but remained much smaller than the microscope field of view. We then took advantage of these specific bead patterns to process P-SHG data exactly in the same ROI of the fascicle at any applied strain (see *yellow ROI* in Fig. 4, *a* and *e*). Fluorescent labeling of the fascicle also served as a depth reference z_0 to locate the fascicle surface.

Fig. 4, *b* and *f*, displays the *x*-polarized SHG mean intensity in the highlighted ROI as a function of the depth within the fascicle and of the incident polarization angle α. These polarimetric diagrams exhibit characteristic features that we attribute to polarization distortions (9):

First, the depth profiles at $\pm\pi/4$ excitation angle display interference fringes with dark spots at ~40 μm depth from tendon surface. These fringes are related to birefringence in the propagation of the laser excitation, which results in a phase delay between the *x*- and *y*-polarization components of the laser excitation. They appear near $\pm\pi/4$ excitation angle because *x* and *y* components have similar amplitudes and destructive interferences are more effective.

Second, the depth profiles at 0 and $\pm\pi/2$ angles are different, which indicates different attenuation lengths within the fascicle for *x*- and *y*-polarization components.

Note that the observed polarimetric diagrams are different at 2% and 4% strains: the dark spots are slightly sharper at 4% strain, whereas attenuation is stronger at 2% strain. We therefore expect quantitatively different parameters ρ after image processing.

Determination of linear and nonlinear anisotropy parameters

These P-SHG data were fitted with a sum of cos $2n\alpha$ functions ($n = 0,1,2$) using Eq. 11. The obtained parameters A,B,C were then used to calculate the SHG anisotropy parameter ρ and the parameter Δ as a function of depth within the tendon (see the Supporting Material). Fig. 4, *c* and *g*, displays raw and corrected values of ρ. The raw ρ-values decrease with increasing depth within the fascicle, whereas ρ is expected to be constant because the fascicle appears as a uniform medium. This artifactual decrease results from diattenuation that accumulates with depth. It is corrected accordingly using Eq. 12 and the diattenuation

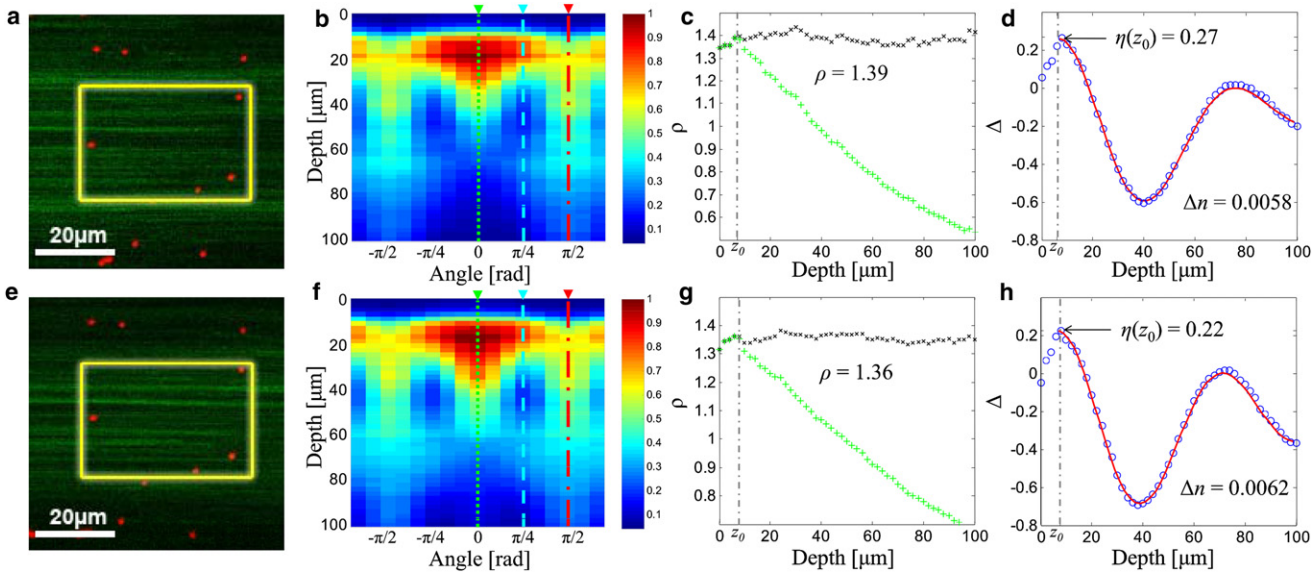

FIGURE 4 P-SHG imaging of the same fascicle at (*a–d*) 2% strain and (*e–h*) 4% strain. (*a* and *e*) Multiphoton images of the tendon fascicle labeled with fluorescent beads. SHG signal (*green color*) is specific for collagen and 2PEF signal (*red color*) reveals the beads. (*Yellow frames*) ROI used for data processing. Fluorescent bead pattern ensures that the same region of the fascicle is processed at any strain. Scale bar: 20 μm. (*b* and *f*) *x*-polarized SHG mean intensity in the highlighted ROI as a function of the incident polarization angle α and of the scanning depth in tendon. (*c* and *g*) Raw (*green*) and corrected (*black*) ρ-value as a function of depth. (*d* and *f*) Δ-value as a function of depth (*blue points*), and fit (*red line*) using Eq. 11 and Eq. S10 in the Supporting Material.

lengths derived from the SHG depth profiles at 0 and $\pi/2$ excitation angles. The corrected ρ then shows a nearly constant value as a function of depth, as expected.

Fig. 4, *d* and *h*, displays the depth profiles of Δ (*blue circles*) as calculated from the P-SHG data. They exhibit oscillations that originate from the fascicle birefringence and reflect the phase shift between *x*- and *y*-polarization components that accumulates along propagation of the laser excitation within the tendon fascicle. The birefringence is then obtained from the position of the first maximum (see the Supporting Material). The decay of the oscillation amplitude is due to the diattenuation. Nonzero value of Δ at $z = z_0$ corresponds to polarization scrambling in the SHG propagation. This effect is nonnegligible at the surface of the fascicle, but vanishes within the tendon because Δ is zero at the next maximum, where there is no contribution from birefringence. The theoretical expression of Δ satisfactorily fits the measured Δ depth profile (see *red lines* in Fig. 4, *d* and *h*). It provides the birefringence value Δn and the polarization scrambling at the fascicle surface $\eta(z_0)$ Here again, we obtain different parameters at 2% and 4% strains; a larger birefringence Δ_n and a smaller cross talk $\eta(z_0)$ are observed at the largest strain.

Variation of fibril orientation distribution with mechanical load

All the optical parameters obtained from P-SHG data are finally displayed as a function of strain in Fig. 5. They all exhibit nonnegligible variations with strain, whether they are linear or nonlinear optical parameters. We obtained similar results for all the tendon fascicles under study. The error bars in Fig. 5 are related to the fitting accuracy and not to the dispersion of different measurements, because this figure displays measurements in the same fascicle at increasing strain. The error bars were calculated using 95% confidence intervals for *A*, *B*, and *C* (data fit using Eq. 11), and taking into account the correlation of these parameters.

The SHG anisotropy parameter ρ decreases from 1.39 to 1.36 while stretching from 2% to 4% and then it increases up to 1.42 (see Fig. 5 *a*). Its average value is in good agreement with our previous measurements (9). Note that ρ was determined at the fascicle surface, where the accumulated phase shift and the diattenuation are zero. The fascicle birefringence Δ_n monotonically increases with strain, going from 0.0058 to 0.0066 (see Fig. 5 *b*). The polarization scrambling at the fascicle surface $\eta(z_0)$ decreases monotonically with strain (see Fig. 5 *c*). Finally, the attenuation lengths for *x*- and *y*-polarized fields also increase monotonically with strain (see Fig. 5 *d*). It means that the fascicle becomes more transparent both for *x*- and *y*-polarized fields when stretched. Diattenuation length is also increasing with strain. Note that the attenuation length for *y*-polarized field is the largest, which means that the tendon fascicle is more transparent for light polarized perpendicularly to the fibrils.

DISCUSSION

Many articles have reported P-SHG comparative studies for different samples, with the aim to use variation of SHG anisotropy parameter ρ to identify different tissues or to find hallmarks of various pathologies (5–8). However, it is not well established yet how this parameter varies within the same tissue as a response to tissue perturbations. To the best of our knowledge, this article reports the first experimental observation of ρ-variations in the same ROI of a collagenous tissue. To that end, we implemented a unique experimental setup that combines P-SHG microscopy with mechanical assays, because mechanical loading is expected to induce a reorganization of the collagen distribution within the tissue. This setup was designed to always monitor the same ROI thanks to symmetric stretching. Accordingly, we successfully visualized the same region of a tendon fascicle that was increasingly stretched up to a few percents and we observed a significant variation of the SHG anisotropy parameter ρ with stretching. Our work then proves that ρ can vary as a function of mechanical load.

However, the SHG anisotropy parameter ρ is not the only optical parameter that is expected to vary upon tissue remodeling. Linear optical parameters may also vary when

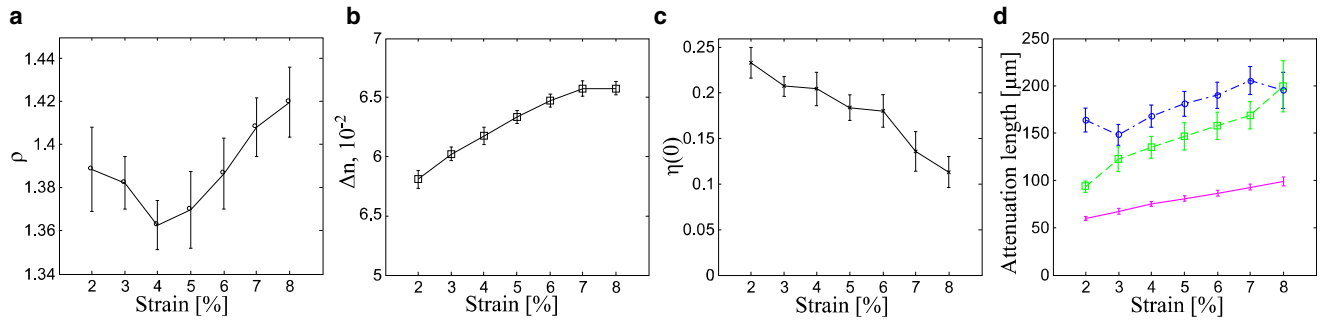

FIGURE 5 Tendon fascicle optical parameters obtained from P-SHG images as a function of strain. (*a*) SHG anisotropy parameter ρ. (*b*) Birefringence Δ_n. (*c*) Polarization scrambling at the fascicle surface $\eta(z_0)$. (*d*) Extraordinary attenuation length (*x* polarization, parallel to the fascicle main axis, *solid line*), ordinary attenuation length (*y* polarization, perpendicular to the fascicle main axis, *dash-dotted line*), and diattenuation length (*dotted line*).

the tendon fascicle is stretched, mainly the birefringence Δn, the diattenuation length Δl, and the polarization scrambling $\eta(z_0)$ near the fascicle surface. Variations of all these parameters are mixed together in the P-SHG response because the polarization state of the excitation beam is modified by birefringence and diattenuation whereas polarization scrambling affects the polarization of the SHG signal. It is therefore mandatory to use an advanced image processing method to separate the variation of the nonlinear optical parameter ρ from the variations of the linear optical parameters Δn, Δl, and $\eta(z_0)$. This approach advantageously enables monitoring of birefringence, diattenuation length, and polarization scrambling as a function of tendon stretching, which provides complementary information about the tissue reorganization at microscopic scale. Most importantly, we obtained reproducible experimental results with error bars small enough to observe significant variations of all the parameters of interest.

These variations with strain have to be related to the tendon microstructure and mechanics. The macroscopic mechanical properties of tendon fascicle have been extensively studied (22–24,30,36). A tendon in its relaxed state is usually considered as a bundle of packed fibrils with a crimped pattern. A mechanism explaining the evolution of the tangent modulus with strain in relationship with the fibril organization has been proposed (22). The initial toe region (see Fig. 3 *b*) is attributed to the straightening of the collagen fibrils. The linear region is then associated with a sliding of the fibrils in their proteoglycan matrix. These two regions correspond to physiological stretching of the tendon fascicle, while the next region showing force saturation at strain beyond 6% is characteristic for nonphysiological disruption of the tendon fascicle. In other words, stretching under physiological conditions is considered to result in a better alignment of the fibrils within the tendon fascicle and is associated with an increase of order and anisotropy of the tissue. Let us discuss in this framework the variations of the linear and nonlinear optical parameters we observed experimentally.

The measured birefringence increases with strain, as expected because the fibrils forming the fascicle become more aligned, increasing the anisotropy that translates into birefringence. It changes by 14% over the full loading path, and by ~7% over the maximal physiological strain range (2–4%).

The same explanation applies to the increase of the attenuation lengths l_x and l_y, but the variations are more dramatic. Thus, l_x exhibits 1.5-fold increase while stretched from 2% to 8%, and l_y exhibits 30% maximal increase. The stretched tendon fascicle with well-aligned fibrils appears to be more transparent for both parallel and perpendicular polarization of the infrared excitation field. The diattenuation length Δl changes even more drastically, displaying twofold increase with strain.

The polarization scrambling $\eta(z_0)$ decreases with strain, as expected if we consider that the surface of an aligned fascicle is smoother and better defined. Scrambling indeed occurs mainly near the surface, and better-aligned fibrils near the surface are expected to scramble the SHG polarization to a smaller extent.

The variation of ρ is not monotonic in contrast to the former parameters. It shows two different regions (see Fig. 5 *a*): ρ first decreases in the interval 2–4% and then rises up from 4% to 8%. This trend was observed for all studied tendons, whether preconditioned or not. The first decreasing part is in agreement with the model we introduced in the theoretical section. It reflects the decrease of ρ with increasing order in tissue, as obtained by the numerical simulation displayed in Fig. 2 *c*. This decreasing behavior corresponds to the heel region on the force-strain curve, which is associated with the physiological range of tendon stretching. It confirms that tendon stretching is associated with a rearrangement of collagen fibrils that results in a better alignment of these fibrils within the tendon fascicle (22–24).

In contrast, the second increasing region of ρ variation with strain indicates that the alignment of collagen fibrils is somewhat disrupted at higher strains. These strains do not correspond to physiological conditions according to the literature (23). This is confirmed by the saturation of the force observed in Fig. 3 *b*. We therefore expect that some fibrils begin to break, resulting in misaligned collagen subfibrils or molecules within the tendon fascicle. Alternatively, this increasing region of ρ at higher strains may be attributed to straightening of the collagen triple-helix itself (37). In this case, the increase of the measured parameter ρ results from variations of ρ_{fib} at the molecular scale, not from orientational changes at the fibrillar scale. We note that a behavior change is also observed to a lesser extent in the birefringence variation that appears to saturate at strains higher than 4%.

Let us now examine the quantitative values obtained for ρ. The range of the measured values for all strains is in good agreement with previous measurements, while the minimal value of ρ provides what to our knowledge is new information about the SHG response of collagen fibrils. This minimal value is obtained typically for 3–4% strains. It corresponds to well-ordered fibrils within the tendon fascicle, so that $\rho \approx \rho_{fib}$ (see Eq. 7 with θ uniformly equal to 0). Our measurements of stretched tendon fascicles thus quantify the SHG anisotropy parameter of collagen fibrils. This parameter is not accessible in relaxed tissues that exhibit a disordered distribution of collagen fibrils, except in the corneal stroma that is the only collagenous tissue with well-aligned fibrils as required for corneal transparency. However, measurements of ρ_{fib} in corneal stroma are less accurate than in stretched tendon fascicles because collagen fibrils are distributed in $\approx$2-μm-thick lamellae. The ρ_{fib} measurements are then significantly disrupted at lamellar interfaces and somewhat along the whole lamellar thickness that approaches the axial optical resolution (13).

An interesting alternative method to measure the SHG anisotropy parameter of collagen fibrils would be to stretch individual collagen fibrils using micromechanical devices (38,39). However, we expect P-SHG signals of single fibrils to be quite small, which would probably deteriorate the accuracy of these measurements. P-SHG imaging in stretched tendon fascicles therefore appears to certainly provide the most accurate measurement of the SHG anisotropy at the fibrillar scale. We obtain $\rho_{fib} = 1.36 \pm 0.01$ for the tendons under study.

This value is related to the orientational distribution of the elementary nonlinear scatterers within the fibrils (3,5,12,27). Considering that these elementary nonlinear scatterers are the peptide bonds and assuming that they all exhibit the same angle Θ to the fibril axis, $\rho_{fib} = 1.36$ gives $\Theta = 50.5^\circ$ by use of Eq. 10. This value is close to the mean orientation of the peptide bonds to the helix axis (45.3° pitch angle). This approach should, however, be refined as suggested recently (12,40,41). It indeed assumes that the elementary nonlinear dipoles are perfectly aligned along the peptide bonds, which has been questioned by quantum chemistry calculations (40). Moreover, side chains or other submolecular units in the amino acids may also contribute to the elementary nonlinear hyperpolarizability (11,12,41). Finally, the interactions between elementary effective nonlinear dipoles along the peptidic sequence may result in strong modifications of the total nonlinear response (12,40). Taking into account all these effects requires advanced theoretical calculations that need to be validated by accurate experimental measurements. In that regard, our measurements show a very good agreement with the value $\beta_{XXX}/\beta_{XYY} = 1.4$ calculated by Tuer et al. (12) by use of ab initio modeling of the first hyperpolarizability of effective amino acids with corrections for pair interactions. Our results then confirm that the P-SHG response in single collagen fibrils is dominated by the orientation of the amino acids in the triple-helical structure.

CONCLUSION

In this article, we showed that the P-SHG response of collagenous tissues mainly reflects the distribution of fibril orientation. For that purpose, we developed a three-scale theoretical approach of the collagen nonlinear optical response: the very elementary scale that corresponds to the nonlinear response of chemical moieties along the amino-acid sequence, the scale of the fibrils that are considered as rigid entities and the scale of the tissue where the fibrils show different orientations that may vary dramatically upon various perturbations. Our calculations indicate that more disordered distributions of fibril orientation in the tissue result in a larger SHG anisotropy parameter ρ. This was confirmed experimentally by stretching a rat-tail tendon fascicle while continuously monitoring ρ in the same ROI of the tissue. We observed unambiguously a decrease of the SHG anisotropy parameter ρ to a minimum value that was attributed to the best alignment of the fibrils at a submicrometer scale. The SHG anisotropy parameter next increased for nonphysiological strains due to the disruption of the tissue. The minimum value of ρ measures the SHG anisotropy parameter at the fibril scale ρ_{fib}. Our measurements thus provide accurate information about the P-SHG response of single collagen fibrils that appear to confirm recent advanced theoretical calculations of the triple helix hyperpolarizability (12).

This approach may be generalized to other mechanical assays to gain insight into the relationship between mechanical loading of collagenous tissues at macroscopic scale and reorganization of collagen fibrils at the microscopic scale. It should also prove efficient to look at wound healing or any tissue remodeling in response to a variety of injuries. P-SHG microscopy coupled to our rigorous image processing and multiscale data analysis will enable measurements of local disorder in the collagen matrix that may reflect pathological processes and provide a quantitative tool for monitoring their progression.

SUPPORTING MATERIAL

A complete description of ρ-calculation and of image processing are available at http://www.biophysj.org/biophysj/supplemental/S0006-3495(12)00409-2.

We gratefully acknowledge G. Liot from Institut Curie, Université Paris XI, for providing us with the rat-tails; V. de Greef, D. Caldemaison, X. Solinas, and J.-M. Sintès for technical implementation of the setup; and G. Latour, M. Zimmerley, F. Hache, and E. Beaurepaire for fruitful discussions.

REFERENCES

1. Stoller, P., K. M. Reiser, …, A. M. Rubenchik. 2002. Polarization-modulated second harmonic generation in collagen. *Biophys. J.* 82: 3330–3342.
2. Williams, R. M., W. R. Zipfel, and W. W. Webb. 2005. Interpreting second-harmonic generation images of collagen I fibrils. *Biophys. J.* 88:1377–1386.
3. Plotnikov, S. V., A. Millard, …, W. Mohler. 2006. Characterization of the myosin-based source for second-harmonic generation from muscle sarcomeres. *Biophys. J.* 90:693–703.
4. Erikson, A., J. Örtegren, …, M. Lindgren. 2007. Quantification of the second-order nonlinear susceptibility of collagen I using a laser scanning microscope. *J. Biomed. Optics.* 12:044002.
5. Tiaho, F., G. Recher, and D. Rouède. 2007. Estimation of helical angle of myosin and collagen by second harmonic generation imaging microscopy. *Opt. Express.* 15:12286–12295.
6. Han, X., R. M. Burke, …, E. B. Brown. 2008. Second harmonic properties of tumor collagen: determining the structural relationship between reactive stroma and healthy stroma. *Opt. Express.* 16:1846–1859.
7. Mansfield, J. C., C. P. Winlove, …, S. J. Matcher. 2008. Collagen fiber arrangement in normal and diseased cartilage studied by polarization sensitive nonlinear microscopy. *J. Biomed. Optics.* 13:044020.
8. Psilodimitrakopoulos, S., D. Artigas, …, P. Loza-Alvarez. 2009. Quantitative discrimination between endogenous SHG sources in

mammalian tissue, based on their polarization response. *Opt. Express.* 17:10168–10176.

9. Gusachenko, I., G. Latour, and M.-C. Schanne-Klein. 2010. Polarization-resolved second harmonic microscopy in anisotropic thick tissues. *Opt. Express.* 18:19339–19352.
10. Aït-Belkacem, D., A. Gasecka, …, S. Brasselet. 2010. Influence of birefringence on polarization resolved nonlinear microscopy and collagen SHG structural imaging. *Opt. Express.* 18:14859–14870.
11. Su, P. J., W. L. Chen, …, C. Y. Dong. 2011. Determination of collagen nanostructure from second-order susceptibility tensor analysis. *Biophys. J.* 100:2053–2062.
12. Tuer, A. E., S. Krouglov, …, V. Barzda. 2011. Nonlinear optical properties of type I collagen fibers studied by polarization dependent second harmonic generation microscopy. *J. Phys. Chem. B.* 115:12759–12769.
13. Latour, G., I. Gusachenko, …, M. C. Schanne-Klein. 2012. In vivo structural imaging of the cornea by polarization-resolved second harmonic microscopy. *Biomed. Opt. Express.* 3:1–15.
14. Campagnola, P. J., A. C. Millard, …, W. A. Mohler. 2002. Three-dimensional high-resolution second-harmonic generation imaging of endogenous structural proteins in biological tissues. *Biophys. J.* 82: 493–508.
15. Zipfel, W. R., R. M. Williams, …, W. W. Webb. 2003. Live tissue intrinsic emission microscopy using multiphoton-excited native fluorescence and second harmonic generation. *Proc. Natl. Acad. Sci. USA.* 100:7075–7080.
16. Strupler, M., A.-M. Pena, …, M. C. Schanne-Klein. 2007. Second harmonic imaging and scoring of collagen in fibrotic tissues. *Opt. Express.* 15:4054–4065.
17. Deniset-Besseau, A., P. De Sa Peixoto, …, M. C. Schanne-Klein. 2010. Nonlinear optical imaging of lyotropic cholesteric liquid crystals. *Opt. Express.* 18:1113–1121.
18. Hulmes, D. J. 2002. Building collagen molecules, fibrils, and suprafibrillar structures. *J. Struct. Biol.* 137:2–10.
19. Parry, D. A. D., and A. S. Craig. 1977. Quantitative electron microscope observations of the collagen fibrils in rat-tail tendon. *Biopolymers.* 16:1015–1031.
20. Roth, S., and I. Freund. 1979. Second harmonic generation in collagen. *J. Chem. Phys.* 70:1637–1643.
21. Nadiarnykh, O., and P. J. Campagnola. 2009. Retention of polarization signatures in SHG microscopy of scattering tissues through optical clearing. *Opt. Express.* 17:5794–5806.
22. Puxkandl, R., I. Zizak, …, P. Fratzl. 2002. Viscoelastic properties of collagen: synchrotron radiation investigations and structural model. *Philos. Trans. R. Soc. Lond. B Biol. Sci.* 357:191–197.
23. Screen, H. R. C., D. L. Bader, …, J. C. Shelton. 2004. Local strain measurement within tendon. *Strain.* 40:157–163.
24. Houssen, Y. G., I. Gusachenko, …, J. M. Allain. 2011. Monitoring micrometer-scale collagen organization in rat-tail tendon upon mechanical strain using second harmonic microscopy. *J. Biomech.* 44:2047–2052.
25. Sage, D. 2011. MIJ: a JAVA package for bi-directional communication and data exchange from MATLAB to ImageJ/Fiji. http://bigwww.epfl.ch/sage/soft/mij/.
26. Butcher, P. N., and D. Cotter. 1990. The Elements of Nonlinear Optics. Cambridge University Press, Cambridge, UK.
27. Deniset-Besseau, A., J. Duboisset, …, M.-C. Schanne-Klein. 2009. Measurement of the second order hyperpolarizability of the collagen triple helix and determination of its physical origin. *J. Phys. Chem. B.* 113:13437–13445.
28. Beck, K., and B. Brodsky. 1998. Supercoiled protein motifs: the collagen triple-helix and the α-helical coiled coil. *J. Struct. Biol.* 122:17–29.
29. Orgel, J. P. R. O., T. C. Irving, …, T. J. Wess. 2006. Microfibrillar structure of type I collagen in situ. *Proc. Natl. Acad. Sci. USA.* 103:9001–9005.
30. Abrahams, M. 1967. Mechanical behavior of tendon in vitro. A preliminary report. *Med. Biol. Eng.* 5:433–443.
31. Hansen, K. A., J. A. Weiss, and J. K. Barton. 2002. Recruitment of tendon crimp with applied tensile strain. *J. Biomech. Eng.* 124:72–77.
32. Screen, H. R. C., J. C. Shelton, …, D. A. Lee. 2005. The influence of noncollagenous matrix components on the micromechanical environment of tendon fascicles. *Ann. Biomed. Eng.* 33:1090–1099.
33. Lacomb, R., O. Nadiarnykh, …, P. J. Campagnola. 2008. Phase matching considerations in second harmonic generation from tissues: effects on emission directionality, conversion efficiency and observed morphology. *Opt. Commun.* 281:1823–1832.
34. Strupler, M., and M.-C. Schanne-Klein. 2010. Simulating second harmonic generation from tendon—do we see fibrils? *Biomed. Optics.* Paper BTuD83.
35. Rivard, M., M. Laliberté, …, F. Légaré. 2010. The structural origin of second harmonic generation in fascia. *Biomed. Opt. Express.* 2:26–36.
36. Fratzl, P. 2003. Cellulose and collagen: from fibers to tissues. *Curr. Opin. Colloid Interface Sci.* 8:32–39.
37. Gautieri, A., S. Vesentini, …, M. J. Buehler. 2011. Hierarchical structure and nanomechanics of collagen microfibrils from the atomistic scale up. *Nano Lett.* 11:757–766.
38. van der Rijt, J. A. J., K. O. van der Werf, …, J. Feijen. 2006. Micromechanical testing of individual collagen fibrils. *Macromol. Biosci.* 6: 697–702.
39. Shen, Z. L., M. R. Dodge, …, S. J. Eppell. 2008. Stress-strain experiments on individual collagen fibrils. *Biophys. J.* 95:3956–3963.
40. Loison, C., and D. Simon. 2010. Additive model for the second harmonic generation hyperpolarizability applied to a collagen-mimicking peptide (Pro-Pro-Gly)10. *J. Phys. Chem. A.* 114:7769–7779.
41. Rocha-Mendoza, I., D. R. Yankelevich, …, A. Knoesen. 2007. Sum frequency vibrational spectroscopy: the molecular origins of the optical second-order nonlinearity of collagen. *Biophys. J.* 93:4433–4444.